Environmental Modelling and Software 171 (2024) 105890

Contents lists available at ScienceDirect

Environmental Modelling and Software

journal homepage: www.elsevier.com/locate/envsoft

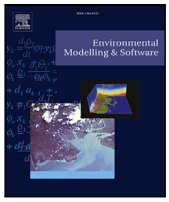

Position Paper

Assessing the hillslope-channel contributions to the catchment sediment balance under climate change

J.P.C. Eekhout [a,*], A. Jódar-Abellán [a,b], E. Carrillo-López [a], C. Boix-Fayos [a], J. de Vente [a]

[a] Soil and Water Conservation Research Group, CEBAS, CSIC, Campus de Espinardo 30100, P.O. Box 164, Murcia, Spain
[b] Centro de Investigación e Innovación Agroalimentaria y Agroambiental (CIAGRO-UMH), Miguel Hernandez University, Ctra. Beniel km 3.2, 03312 Orihuela, Spain

ARTICLE INFO

Keywords:
Hillslope erosion
Channel erosion
Climate change impact
Land use change
Sediment budget
Large-scale modelling

ABSTRACT

To get a full understanding of the impacts of global change on the catchment-scale sediment balance, models are needed that combine hillslope soil erosion processes with channel morphodynamics. Here we present a modification to the SPHY-MMF model that includes a novel channel morphodynamics module, which determines erosion and deposition in rills and channels. We applied the model to a Mediterranean study area in southeast Spain, in which we show that channel erosion contributes substantially (35%–40%) to the total sediment yield, highlighting the importance of accounting for channel erosion in catchment-scale sediment budget estimations. The climate change scenarios show that the different erosional processes (i.e. sheet, rill, channel) are projected to decrease or increase, depending on the projected change in annual and extreme precipitation. From this we conclude that interactions between different erosional and depositional processes should be considered when studying the impact of global change on the catchment-scale sediment balance.

1. Introduction

Soil erosion is one of the principal forms of soil degradation (Koch et al., 2013), affecting the fertile top soil layer, which plays an essential role in agricultural productivity and is fundamental for the provision of food security (Amundson et al., 2015). At large spatial scales, soil erosion is assessed using models, which allow to evaluate the impact of land use and climate change on soil loss and the adaptation potential of soil conservation measures (Eekhout and de Vente, 2022). Most soil erosion models simulate hillslope erosion processes, such as sheet and rill erosion (Morgan, 2005) and account for the on-site impacts on soil fertility. Sediment transport models are used to assess the off-site impacts on the catchment-scale sediment balance, for instance, to assess the impacts on reservoir storage capacity loss (de Vente et al., 2005). However, river channels, which we define as the main channel and adjacent floodplain, may also be an important source or sink of sediment (de Vente et al., 2007), which is hardly ever considered in soil erosion impact assessments, due to the difficulties to measure or predict channel erosion and deposition at large spatial scales. Moreover, it is likely that catchment-scale soil erosion model assessments often overestimate hillslope erosion rates when they are calibrated with sediment yield estimates taken at the catchment outlet (de Vente et al., 2013). To overcome these limitations, here, we present a soil erosion model coupled with a newly developed channel morphodynamics model. To demonstrate its functionality and identify remaining research needs, we apply the model to assess the impact of land use and climate change on the catchment sediment balance, considering the most relevant catchment-scale sediment sources and sinks.

Soil erosion on hillslopes can be caused by two interrelated processes, i.e. detachment by raindrop impact and detachment by runoff (Morgan, 2005). Soil erosion occurs when raindrops hit the soil surface and detach sediment particles in the process, which is often referred to as raindrop splash erosion (Morgan, 2005). On the upstream part of hillslopes and in interrill areas, detachment by runoff is mostly characterized by sheet erosion. When enough water accumulates, rills are formed on the hillslope (Govers et al., 2007), which become (ephemeral) gullies and eventually channels when more water accumulates over longer distances (Vanmaercke et al., 2021). In all cases (i.e. sheet, rill, gully or channel erosion), detachment by runoff is a function of the flow velocity or discharge, which are mostly determined by flow depth and slope. The amount of soil erosion is furthermore determined by the erodibility of the soil, vegetation characteristics and land management practices (Morgan, 2005; Martínez-Mena et al., 2020), in which a densely vegetated soil is better able to retain the soil than sparsely vegetated soils (Maetens et al., 2012a).

Soil erosion models are needed to simulate the impact of global change (i.e. climate and land use change) on soil loss and its implications for the loss of soil fertility, land degradation, and eventually food

* Corresponding author.
E-mail address: joriseekhout@gmail.com (J.P.C. Eekhout).

https://doi.org/10.1016/j.envsoft.2023.105890
Received 2 June 2023; Received in revised form 10 November 2023; Accepted 13 November 2023
Available online 15 November 2023

security. Soil erosion models can be subdivided into models forced by precipitation only, by runoff only, or by both precipitation and runoff (Eekhout and de Vente, 2020). Models forced by precipitation only, such as RUSLE (Renard et al., 1997), are not capable of simulating rill and gully erosion, because of the lack of (accumulated) runoff processes accounted for in these models. Models forced by runoff only, such as MUSLE (Williams, 1975) and PESERA (Kirkby et al., 2008), do simulate these runoff processes and, hence, are able to simulate rill and potentially gully erosion, however, they lack the precipitation forcing to simulate raindrop splash erosion. Models that are forced by both precipitation and runoff, such as WEPP (Nearing et al., 1989) and MMF (Morgan and Duzant, 2008), incorporate both detachment processes and can potentially simulate all relevant soil erosion processes that occur on the hillslopes. Therefore, these models can give useful insights on the specific hillslope soil erosion processes and can be used to assess the impact of global change on soil loss at the hillslope scale, while accounting for all relevant soil erosion processes.

Soil erosion does not only have on-site impacts, but there are also relevant off-site impacts, including channel morphodynamics and sedimentation of reservoirs (Vörösmarty et al., 2003; Poesen, 2018). Sediment delivery ratios (SDR) are often used in combination with USLE-type of models to determine the amount of sediment that is delivered to the catchment outlet (de Vente et al., 2007). In most cases, an SDR smaller than 1 is assumed, which means that soil erosion from the hillslopes accounts for all the sediment eroded in a particular catchment and is partly deposited at local depressions, parcel boundaries, footslopes, or floodplains. However, de Vente et al. (2008) showed that often not all sediment yield at the catchment outlet can be explained by the contribution of soil erosion from the hillslopes alone, hence, other sources should be considered, as well. This is particularly true for Mediterranean environments, where gully and channel erosion may significantly contribute to the catchment-scale sediment balance (Lagacherie et al., 2018). Their contribution generally increases when considering larger spatial scales (de Vente et al., 2007; Govers, 2011), hence, large-scale studies should particularly consider these extra sources and sinks of sediment.

Field studies have shown that river channels may have a significant contribution to the catchment-scale sediment balance (e.g. Trimble, 1997; Ben Slimane et al., 2016). River channels may act as a source in the case of channel incision and bank erosion. Channel incision occurs when the flow of water above the channel bed is high enough that sediment particles are entrained into the water column (Aksoy and Kavvas, 2005). Bank erosion occurs when similar processes occur at the channel bank, especially due to secondary flow dynamics in river bends (Langendoen and Simon, 2008). In-channel morphodynamics and (temporary) sediment deposition in channels may also play an important role, where channel beds can be covered by channel bars, which can migrate, grow in amplitude and disappear, even within one flood event (Eekhout et al., 2013).

Climate change will affect channel morphodynamics as a result of the projected changes in the discharge regime (Lotsari et al., 2015) and can be assessed by the application of hydraulic models equipped with sediment transport equations and channel morphodynamics formulations (Camporeale et al., 2007). With increasing complexity, channel morphodynamic models may simulate the three dimensional development of the channel bed, however, because of high data and computational demands, such models are in most cases only applied to river reaches of a few river meanders (Ikeda et al., 1981). 1D-morphodynamic models are applied to simulate catchment-scale channel morphodynamics in the entire channel network (e.g. Tangi et al., 2019; Bizzi et al., 2021). These models do not incorporate all morphological processes and are often restricted to simulate changes in the channel bed, including incision and sedimentation, without considering bank erosion and in-channel morphodynamics. The transport capacity of the flow is often used to determine whether erosion or deposition takes place, which is a function of the flow conditions (e.g. flow velocity) and a critical value for transport to occur (e.g. critical shear stress) (Wainwright et al., 2015). Channel sedimentation occurs when the input of sediment is higher than the transport capacity, while channel erosion occurs in the opposite case.

To assess the impacts of climate and land use change on the catchment-scale sediment balance, models are needed that combine hillslope soil erosion processes with channel morphodynamics (de Vente et al., 2007, 2013; Poesen, 2018). Process-based soil erosion models combined with sediment transport equations allow such assessments, but are often only applicable at small spatial scales (Batista et al., 2022). The objective of this study is to develop a soil erosion model coupled with a channel morphodynamics model that can be applied to assess the impacts of global change on sediment budgets at large spatial scales. Therefore, we present a modification to the process-based SPHY-MMF model, which has proven to be applicable at large spatial scales that are most relevant for policy makers (e.g. Eekhout et al., 2018a; Eekhout and de Vente, 2019a; Eekhout et al., 2020). Furthermore, we illustrate the capabilities of this new model and the remaining needs for further model development through model applications in a Mediterranean catchment in southeast Spain, with (1) a focus on historical land use change and check dam construction and (2) an assessment of the impact of climate change on the catchment-scale sediment balance.

2. Model description

SPHY-MMF (Eekhout et al., 2018b) is a spatially distributed model that simulates hydrological and soil erosion processes on a cell-by-cell basis and is applied at a daily time step. The model is written in the Python programming language using the PCRaster dynamic modelling framework (Karssenberg et al., 2010). To allow evaluation of the impacts of global change on catchment scale sediment budgets, here we present a modification to the SPHY-MMF model, which includes the implementation of a new water routing algorithm, a modification of the sediment transport module and a novel channel morphodynamics module.

2.1. Hydrological model

SPHY-MMF is a spatially distributed "leaky bucket" type model that simulates the most relevant hydrological processes, including interception, evapotranspiration, evolution of vegetation cover, surface runoff, and lateral and vertical soil moisture flow. Here we give a summary of the hydrological processes accounted for by the SPHY-MMF model. A full description can be found in Terink et al. (2015).

SPHY-MMF is forced by daily precipitation and temperature (average, minimum and maximum) data, for which the temperature data are used to determine the reference evapotranspiration through the Hargreaves equation (Hargreaves and Samani, 1985). The potential evapotranspiration is obtained by multiplying the reference evapotranspiration by the crop coefficient, which is obtained from a linear relationship with the Normalized Differenced Vegetation Index (NDVI) from the vegetation module. The vegetation module also determines the leaf area index (LAI), canopy storage and interception. The actual evapotranspiration is obtained by multiplying the potential evapotranspiration with a soil water deficit/surplus factor, which is a function of soil hydraulic properties, the current soil water content and plant-specific water need. Surface runoff is simulated by infiltration excess and saturation excess processes, where the former is obtained by a daily implementation of the Green–Ampt equation (Heber Green and Ampt, 1911) and the latter as a function of the actual and saturated water content. The model accounts for three soil layers, i.e. root-zone, subzone and groundwater layer. Water can percolate from the root-zone to the subzone to the groundwater layer. Capillary rise may occur between the subzone and the root-zone. The total runoff consists of

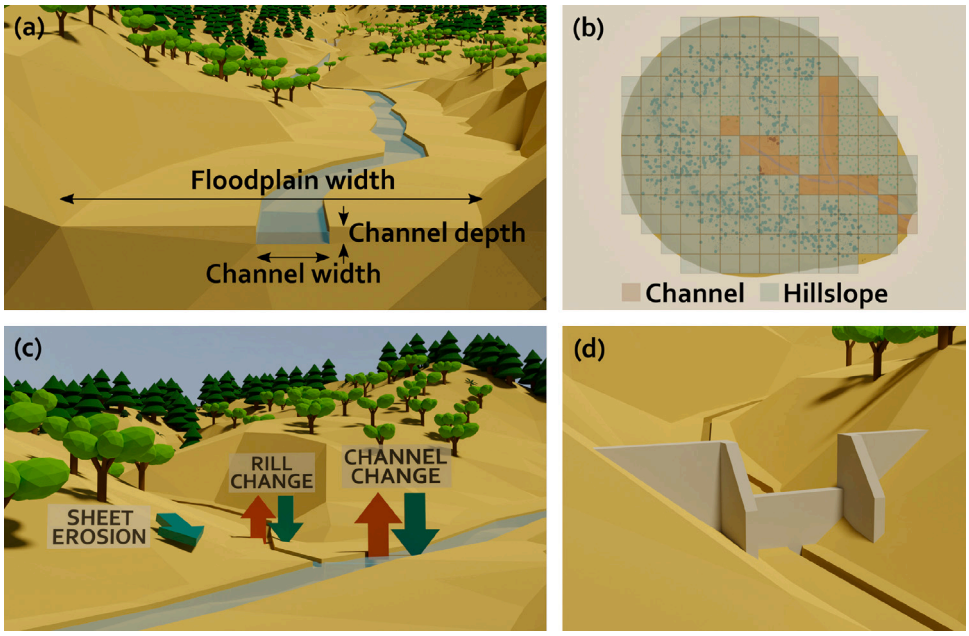

Fig. 1. Description of the SPHY-MMF model: (a) channel cross-section, (b) channel and hillslope grid cells within the model domain, (c) erosion and deposition processes, and (d) example of a check dam.

the sum of surface runoff, lateral flow from the root-zone and baseflow from the groundwater layer.

The original SPHY-MMF model simulated the routing of water using a single flow algorithm, where a flow recession coefficient accounted for the flow delay from channel friction. Here we present a new water routing module that is based on a travel time algorithm. This algorithm determines the discharge in each grid cell given the spatially distributed channel storage and flow velocity. Channel dimensions are needed to determine the channel storage and flow velocity, which are based on a rectangular channel cross-section, including a floodplain (Fig. 1a). The channel storage is defined as the amount of water that is available within the channel cross-section for routing and is obtained from the sum of the channel storage of the previous time step and the total runoff generated within each cell from the current time step. The flow velocity is obtained using an iterative process, in which the flow velocity (u) is determined using the Manning's equation:

$$u = \frac{R^{2/3} S^{1/2}}{n} \tag{1}$$

where R is the hydaulic radius (m), S the slope (m m^{-1}) and n the Manning roughness coefficient (s m$^{-1/3}$). Through the travel time algorithm, the obtained flow velocity is used to determine the discharge, which is, subsequently, compared with the discharge of the previous iteration. Once the difference in all grid cells is smaller than a threshold parameter (here set to 0.01 m^3 s^{-1}) the iteration finishes and spatially distributed discharge and flow velocity maps are obtained for the current time step. The new water routing algorithm requires channel dimensions as input, including channel depth, channel width and floodplain width. In the cells where the water depth exceeds the channel depth, a compound Manning roughness n_{compound} is obtained using the Lotter method, which accounts for the channel and floodplain dimensions and roughness values and shows the least error compared to other compound channel methods (Motayed and Krishnamurthy, 1980) (see Text S1).

It is assumed that each cell consists of a channel and a floodplain, hence, the channel dimensions need to be defined for each cell, which can consist of single parameter values or spatially distributed maps. As an alternative, the study area can be subdivided into channel and hillslope cells (Fig. 1b), where the channel dimensions are only applied to the channel cells, while rills are assumed on the hillslope cells. The rill dimensions are assumed to be square shaped (i.e. rill width is equal to rill depth) and are defined by a minimum and maximum rill width/depth, which are linearly interpolated from the most upstream located hillslope cells towards the hillslope cells that have the largest upstream area. The subdivision between channel and hillslope cells is particularly interesting for the simulation of sediment transport and morphodynamics of rills and channels, as explained below.

The model currently accounts for re-infiltration (Zhang et al., 2020) from the channels to the root zone, which occurs only when the channel storage is larger than 0. If this is the case, the model determines if water is present in the floodplain or in the channel only. Given the area that is covered by water (i.e. the channel and/or floodplain area), the model determines the potential re-infiltration assuming an infiltration capacity equal to the saturated hydraulic conductivity. Re-infiltration is equal to the potential re-infiltration if it does not exceed the current channel storage, otherwise re-infiltration is equal to channel storage. In the case the root zone is not saturated, re-infiltration is subsequently added to the root water content and subtracted from the channel storage.

2.2. Soil erosion model

Soil erosion is determined using a daily implementation of the Morgan–Morgan–Finney model (MMF; Morgan and Duzant, 2008), which simulates the most relevant soil erosion processes, including detachment by raindrop impact, detachment by runoff and immediate deposition. Here we give a summary of the soil erosion processes accounted for by the daily implementation of the MMF model, please see Eekhout et al. (2018b) for a full description of these processes.

Detachment of soil particles is determined for each sediment class (clay, silt, sand) separately by two processes, i.e. raindrop impact and runoff. Detachment by raindrop impact (F_i) is a function of the kinetic energy of the effective precipitation KE:

$$F_i = K_i \frac{\%i}{100}(1 - GC)KE \times 10^{-3} \tag{2}$$

where K is the detachability of the soil by raindrop impact (g J^{-1}), i is the textural class (-), GC is the ground cover (-), and KE is the kinetic energy of the effective precipitation (J m^{-2}), which is the sum of the kinetic energy of direct throughfall and leaf drainage. The detachability

of the soil for each texture class is included as a model parameter, for which (Quansah, 1982) proposed $K_c = 0.1$, $K_z = 0.5$ and $K_s = 0.3$ g J^{-1}, for clay (c), silt (z) and sand (s), respectively.

Detachment by runoff (H_i) is a function of runoff Q, which in the current version of the model is the local runoff. In the previous version of the model (Eekhout et al., 2018b), detachment by runoff was forced by accumulated runoff, to simulate rill and channel erosion, which in the current version is simulated by the novel morphodynamics module, see below. Detachment by runoff is determined as follows:

$$H_i = DR_i \frac{\%i}{100} Q^{1.5} (1 - GC) \sin^{0.3} S \times 10^{-3} \quad (3)$$

where DR is the detachability of the soil by runoff (g mm^{-1}) and Q is the runoff (mm). The detachability of the soil for each texture class is included as a model parameter for which Quansah (1982) proposed $DR_c = 1.0$, $DR_z = 1.6$ and $DR_s = 1.5$ g mm^{-1}, for clay (c), silt (z) and sand (s), respectively.

The soil erosion model simulates immediate deposition DEP (%), which is estimated from a relationship obtained by Tollner et al. (1976) and calculated separately for each texture class:

$$DEP_i = 44.1 N_{f_i}^{0.29} \quad (4)$$

where N_f is the particle fall number (-), which is a function of the flow velocity of the surface runoff. The flow velocity is obtained from the Manning's equation. The roughness that is needed for this equation is a combination of soil and vegetation roughness. The soil roughness can be defined by bare soil or tilled soil roughness, here assumed 0.015 and 0.045 s $m^{-1/3}$, respectively. The vegetation roughness can either be based on a function of stem diameter and density (Jin et al., 2000), which is most appropriate for regular vegetation patterns (e.g. in agricultural fields), or a single parameter value, which is most appropriate for irregular vegetation patterns (e.g. in natural areas). The detached soil that is not deposited is taken into transport.

2.3. Sediment transport model

Sediment transport is determined by the transport capacity separately for the hillslopes (rills) and channels, using the Govers (1990) and Yalin (1963) transport capacity equations, respectively. For both cases, the sediment transport capacity is determined per sediment class, i.e. clay, silt, sand and gravel. The model allows to set a maximum allowable sediment concentration to prevent unrealistic sediment transport capacity. Here we assume a maximum sediment concentration of 1060 g l^{-1}, following Hessel and Jetten (2007). The obtained transport capacity (g l^{-1}) is multiplied by the daily discharge to obtain the daily sediment transport (t day^{-1}).

2.3.1. Hillslope sediment transport

On the hillslopes we implemented the Govers (1990) equation, which was originally obtained through flume experiments, simulating a hillslope under varying angles and using different discharge rates. The Govers (1990) equation has previously been implemented in other process-based soil erosion models, such as EUROSEM (Morgan et al., 1998) and LISEM (De Roo et al., 1996). The transport capacity is determined as follows:

$$TC = \frac{TC_f}{1 - \frac{TC_f}{\rho_s}} \quad (5)$$

where TC is the transport capacity (g l^{-1}), TC_f is the 'dirty water' transport capacity (g l^{-1}) and ρ_s is the sediment density (kg m^{-3}). The 'dirty water' transport capacity is determined as follows:

$$TC_f = c(\omega - \omega_{cr})^d \rho_s \quad (6)$$

where ω and ω_{cr} are the unit stream power and critical unit stream power (cm s^{-1}), respectively, and c and d are functions of the median grain size:

$$c = \left(\frac{D_{50} + 5}{0.32} \right)^{-0.6} \quad (7)$$

$$d = \left(\frac{D_{50} + 5}{300} \right)^{0.25} \quad (8)$$

where D_{50} is the median grain size (μm).

The unit stream power ω is determined as follows:

$$\omega = 100 u S \quad (9)$$

where u is the flow velocity (m s^{-1}) and S is the slope (m m^{-1}). The critical unit stream power ω_{cr} is assumed to be 0.4, according to Govers (1990).

2.3.2. Channel sediment transport

In the channels we implemented the Yalin (1963) equation, which simulates bed load transport in channels. The Yalin (1963) equation is a widely used sediment transport equation, implemented in other process-based soil erosion models, such as WEPP (Nearing et al., 1989) and CREAMS (Knisel, 1980). Transport capacity is determined according to:

$$TC = \frac{q_b w}{Q} \quad (10)$$

where q_b is the volumetric bedload transport per unit width (m^2 s^{-1}), w is the flow width (m) and Q is the discharge (m^3 s^{-1}). The volumetric bedload transport is determined as follows:

$$q_b = (\rho_s - \rho) D_{50} U_* P \quad (11)$$

where ρ is the water density (kg m^{-3}), U_* is the shear velocity (m s^{-1}) and P is a function of the Shields parameter (-). The shear velocity U_* is given by:

$$U_* = \sqrt{gRS} \quad (12)$$

where g is the gravitational acceleration (m s^{-2}) and R is the hydraulic radius (m). The Shield parameter dependent function P is defined by:

$$P = 0.635 \frac{Y}{Y_{cr} - 1} \left(1 - \frac{\ln(1 + ar)}{ar} \right) \quad (13)$$

where Y and Y_{cr} are the Shields parameter and critical Shields parameter (-), respectively, and ar is defined as follows:

$$ar = \frac{2.45}{S^{0.4}} \sqrt{Y_c r \left(\frac{Y}{Y_{cr} - 1} \right)} \quad (14)$$

The Shields parameter Y is defined by:

$$Y = \frac{RS}{D_{50}(s - 1)} \quad (15)$$

where $s = rho_s / rho$ is the ratio between the sediment and water density (-). The critical Shields parameter Y_{cr} is assumed to be 0.06 according to Yalin (1963).

2.4. Channel morphodynamics

The channel morphodynamics module determines the amount of erosion and deposition in the rills and channels (Fig. 1c) using an algorithm that determines the accumulation and detachment of material in the drainage network, considering the transport capacity of the flow. The algorithm requires three input datasets, i.e. the local drainage direction, the amount of available sediment taken into transport and the transport capacity of the flow. The amount of available sediment is the sum of the sediment taken into transport, as determined by the soil erosion module, and the amount of sediment available in the rills and the channels. The latter is obtained as follows:

$$Sed_{\text{store},i} = \frac{\%i}{100} d_{\text{bed}} w l \rho_s 10^{-3} \quad (16)$$

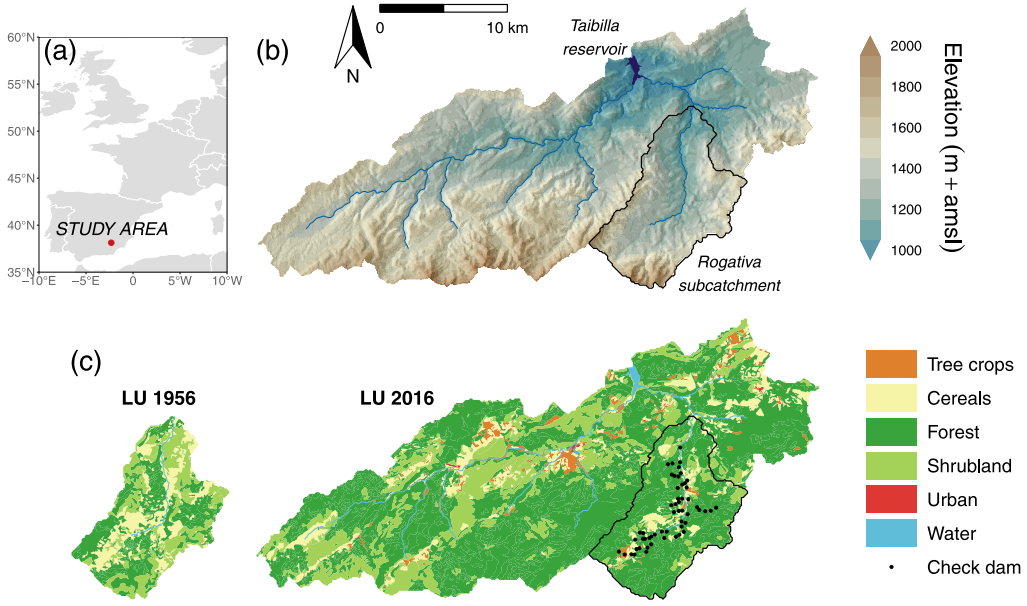

Fig. 2. (a) Location of the Upper Taibilla catchment in Europe, (b) Digital Elevation Model of the study area, including the location of the Taibilla reservoir, the channel network and the Rogativa subcatchment, and (c) land use maps for the years 1956 (only for Rogativa subcatchment) and 2016, where the latter land use map also includes the location of the 58 check dams in the Rogativa subcatchment.

where $Sed_{\text{store},i}$ is the sediment store for sediment class i (Mg), $\%i$ is the fraction of sediment class i (%), d_{bed} is the rill/channel bed thickness (m), w is the rill/channel width (m) and l is the cell length (m). The rill and channel bed thickness d_{bed} is determined as a fraction of the rill and channel depth, respectively, for which two parameters are included in the model.

The morphodynamics algorithm is applied for each of the four sediment classes (i.e. clay, silt, sand and gravel), where the amount of available sediment is proportional to the fraction of each sediment class ($\%i$). On the hillslopes the sediment fraction is obtained from the spatially distributed sediment texture maps, which include clay, silt and sand. The channels include a gravel fraction, which is assumed to be absent on the hillslopes. The four sediment fractions in the channels should be defined using a spatially distributed input map or as fixed values for the entire channel network. For stability reasons, the sediment store is kept constant throughout the simulation period. Hence, the model does not simulate changes in channel dimensions, e.g. channel incision, but projects the amount of rill/channel erosion or deposition, without updating the rill/channel dimensions based on these estimates.

The channel morphodynamics module accounts for sedimentation of hydraulic structures, such as large reservoirs and check dams (Fig. 1d). Each hydraulic structure requires a trapping efficiency (%), which determines the fraction of sediment that is retained behind the structure and the fraction that continues its way in downstream direction.

3. Model application

To illustrate the model performance, its functionality, and its capacity for use in global change scenario studies, we applied the model to a Mediterranean study area in southeast Spain, to assess the impact of (1) historical land use change and check dam construction, and (2) future climate change on the catchment-scale sediment balance, differentiating between different sources (i.e. sheet, rill and channel erosion) and sinks (i.e. rill and channel deposition and check dam/reservoir sedimentation).

3.1. Study area

We applied the model to the Upper Taibilla catchment (315.9 km^2; Fig. 2), which is characterized by a Mediterranean climate, with an average annual precipitation of 555 mm (1991–2020; Peral García et al., 2017). Land use in the study area (Fig. 2c) is dominated by natural vegetation (68% forest and 21% shrubland), while a less significant fraction of the study area is occupied by rainfed agriculture (11%). A reservoir with a capacity of 9 Hm^3 is located at the catchment outlet (Fig. 2b).

Land use change in the past 60 years is characterized by reforestation (Fig. 2c), which had some positive impacts on ecosystem services, such as a decrease of flood discharge and soil erosion (Boix-Fayos et al., 2020; Eekhout et al., 2020). In some parts of the catchment (mainly in the Rogativa subcatchment), reforestation (green infrastructure) was accompanied with the construction of check dams (grey infrastructure), to prevent sedimentation of the Taibilla reservoir. The combination of these two measures caused a decrease of soil erosion and changes to the channel morphodynamics, including channel incision and bank erosion (Boix-Fayos et al., 2007, 2008). The current channel is defined by a single-thread low-sinuous meandering channel planform, including dynamic channel bars. The bed material consists of a mixture of gravel and coarse sand.

3.2. Land use change and check dam construction scenarios

We applied the model to a historical land use change and check dam construction scenario in the Rogativa subcatchment (54.04 km^2). We applied the model to two catchment configurations: (1) the land use of 1956 for the period 1953–1982, without considering the check dams, and (2) the land use of 2016 for the period 1991–2020, considering the check dams that were built in 1976 and 1977. The characteristics and locations of the check dams were obtained by Boix-Fayos et al. (2007). While 58 check dams were constructed in the Rogativa catchment, here we only consider 55 check dams, because several check dams were located in the same cell in the model domain and the model only allows to simulate 1 check dam per cell. In those cases, we included the check

Table 1
Precipitation sum (mm) and extreme precipitation (mm) for the reference and two future climate scenarios. Extreme precipitation is defined as the 95th percentile of daily precipitation, considering only rainy days (>1 mm day^{-1}; Jacob et al., 2014). Values in italic indicate significant changes ($p < 0.05$) with respect to the reference scenario.

Scenarios	Precipitation sum (mm)	Extreme precipitation (mm)
Reference	554.6	18.8
+1.5 °C	560.0 (1.0%)	*21.1 (12.3%)*
+3.0 °C	*483.2 (−13.7%)*	*20.6 (4.3%)*

dam with the highest trapping efficiency. The trapping efficiency (TE) of the check dams was based on (Brown, 1943):

$$TE = \left(1 - \frac{1}{1 + 0.0021\frac{V}{A*0.01}D}\right)100 \quad (17)$$

where V is the volume of the area behind the check dam where sediment can be stored, A is the drainage area behind the check dam, and D is a constant, which we assumed to be 0.76, following Boix-Fayos et al. (2008). The historical climate data were obtained from a 5-km gridded dataset from the Spanish national meteorological institute (AEMET; Peral García et al., 2017). Land use was obtained by aerial photo interpretation for 1956 and 2016, applying a digitization scale of approximately 1:5000 (Eekhout et al., 2020).

3.3. Climate change scenarios

We applied the model to a future climate change scenario in the Taibilla catchment. We applied the model to a reference scenario (1991–2020) and two future climate scenarios, based on +1.5 and +3.0 °C global mean temperature rise. Climate data for the reference scenario were obtained from a 5-km gridded dataset from the Spanish national meteorological institute (AEMET; Peral García et al., 2017). Climate data for the future climate scenarios were obtained from nine GCM/RCM (General Circulation Model/Regional Climate Model) combinations from the EURO-CORDEX initiative (Jacob et al., 2014), with a 0.11° resolution, for the RCP8.5 Representative Concentration Pathway (Table S1). The two temperature scenarios were prepared as follows. We applied the method by Vautard et al. (2014) to determine the year when the five GCMs reach the defined increase in global mean temperature relative to preindustrial levels (1881–1910) and used the 30-year periods centred around these years as input for the model (Table S1). The RCM data were bias-corrected using Scaled Distribution Mapping (Switanek et al., 2017), which gives the best results with respect to other bias-correction techniques applied in the study area, especially considering representation of extreme events (Eekhout and de Vente, 2019b). Before applying bias correction, the climate model data were interpolated onto the 5-km reference climate grid, using linear and spline interpolation for precipitation and temperature, respectively. The two climate change scenarios considered here are characterized by an increase in extreme precipitation (+1.5 °C) and simultaneous decrease in annual precipitation and increase in extreme precipitation (+3.0 °C), with respect to the reference scenario (Table 1 and Figure S1).

We accounted for climate model uncertainty by applying a paired U-test (Mann–Whitney–Wilcoxon test, with a significance level of 0.05). The paired U-test was used to determine the significance of the spatially distributed model outcomes, in which the pairs consisted of the model outputs for (1) the reference scenario and (2) the nine climate models. The paired U-test was also applied to determine the significance of the changes in the catchment sediment balance with respect to the reference scenario.

3.4. Input data

Apart from the climate data, the model requires other input data. The channel network was defined by a dataset from the local water authority (Confederación Hidrológica del Segura). The channel dimensions were obtained using a combination of a LiDAR-based digital elevation model with a 2 m resolution and aerial photos with a 0.25 m resolution (Ministerio de Fomento de España, 2015). We obtained bankfull channel width and depth estimates at 20 transects throughout the channel network, in which we averaged the channel dimensions from 5 repetitions at each transect. The channel widths were obtained by aerial photo interpretation and were defined by the width between the two channel banks, as defined by the location where riparian vegetation starts. The channel depth was obtained by the difference between the lowest point between the channel banks and the average channel bank elevation, obtained from the LiDAR dataset. This method was validated with field measurements of bankfull channel dimensions obtained in 10 transects, with 5 repetitions per transect and gave satisfactory results. On hillslopes, the rills were estimated to have minimum and maximum dimensions (rill width and depth) of 0.05 m and 0.3 m, respectively (Knighton, 1998).

All input maps were interpolated or resampled to the 200 m model resolution. The digital elevation model was obtained from a Spanish national LiDAR dataset (Ministerio de Fomento de España, 2015) with a 5 m resolution. Soil texture (clay, silt, sand) and organic matter were obtained from the SoilGrids dataset (Hengl et al., 2017). The spatially distributed rock fraction map was obtained by applying the empirical formulation from Poesen et al. (1998), which determines rock fraction based on slope gradient.

Channel bed material was obtained in 8 channel reaches distributed over the study area, which included 5 repetitions in each channel reach. The bed material samples were taken up to 5 cm below the bed surface. The obtained sediment samples were oven-dried at 105 °C for 24 h. The sediment fractions were obtained by weighting the amount of sediment per sieve, differentiating between fine sediment (<0.063 mm), sand (0.063–2 mm) and gravel (>2 mm). We did not differentiate between clay and silt, because of the low amount (~1%) of fine sediment obtained from the sediment samples. We therefore divided the fraction of fine sediment equally over the clay and silt classes (i.e. each 50% of the fine sediment fraction). We used the median of the sediment fraction distributions obtained from the 8 channel reaches as input for the model simulations, i.e. 68.5% gravel, 30.3% sand, 0.6% silt and 0.6% clay.

NDVI images were obtained from bi-monthly Moderate Resolution Imaging Spectroradiometer (MODIS; Didan, 2015) data for the period 2001–2016. No NDVI images were available for the historical and future periods considered in this study. Therefore, we separated the NDVI data into inter- and intra-annual NDVI estimates, which were combined to obtain NDVI time series needed for the model runs. To determine the inter-annual NDVI we applied a land use specific log-linear regression model based on annual precipitation and temperature time series, as described in detail in Eekhout et al. (2018b). The intra-annual NDVI was obtained from the long-term average bi-monthly (16 day) NDVI for the period 2001–2016, also differentiated per land use class.

3.5. Model calibration

Model calibration consisted of three parts: hydrology, soil erosion and sediment transport/channel morphodynamics. First, the hydrological part of the model was calibrated using daily discharge data obtained at the Taibilla reservoir for the period 2001–2019. The reservoir inflow time series were obtained by solving the reservoir water balance, consisting of the daily time series of measured reservoir outflow and storage and corrected for estimated reservoir evaporation. The reservoir evaporation was estimated by applying the Hargreaves

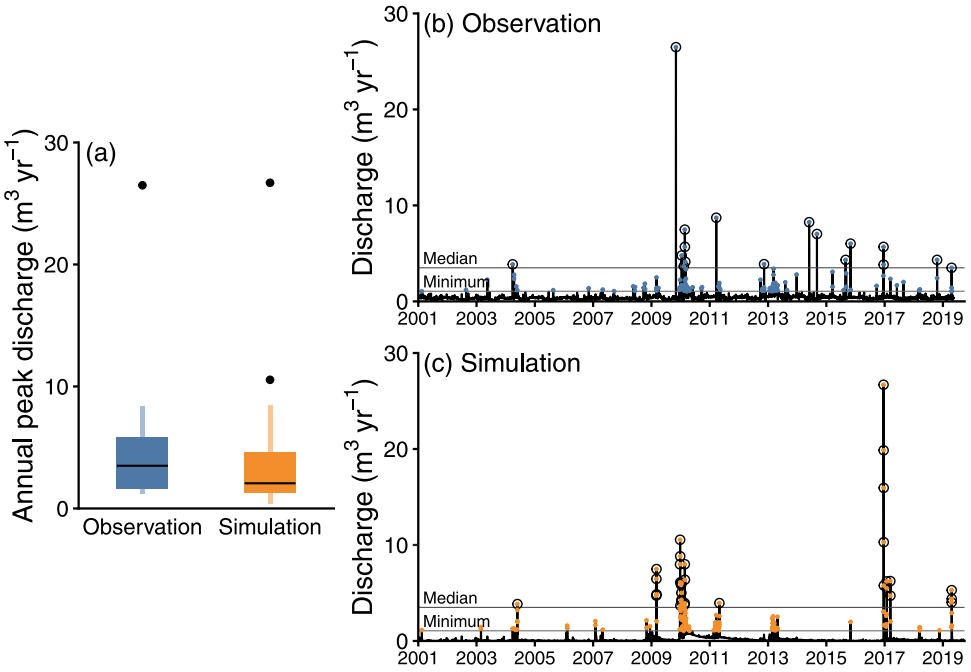

Fig. 3. (a) Distribution of annual maximum discharge for the observed and simulated model run. The coloured boxes indicate the inter-quantile range (25th and 75th percentiles), the black line the median (50th percentile) and the whiskers extend to the 10th and 90th percentiles. The discharge time series of the observations (b) and simulations (c), highlighting the occurrences of discharge higher than the minimum and median annual peak discharge.

equation (Hargreaves and Samani, 1985), using a temperature time series obtained at a nearby climate station. Initially, we attempted to calibrate the model using the observed and simulated discharge time series. However, this resulted in too much discrepancy between the two time series, especially with respect to the timing and intensity of the peak discharges. The large differences between the observed and simulated time series may be related to possible anthropogenic influences and the combination of karst and groundwater inflow from adjacent catchments (Jodar-Abellan et al., 2018). Hence, we decided to focus the hydrological calibration on the intensity and frequency of peak discharges, rather than on the time series themselves. The intensity of the peak discharges was quantified by the distribution of the annual maximum discharge (n = 19). We then compared the observed and simulated distribution of annual maximum discharges using the non-parametric Wilcox-test. Satisfying calibration results were obtained with a p-value > 0.05, meaning that no significant differences were present between the observed and simulated distributions. The frequency of the peak discharges was quantified by the frequency of discharges greater than the observed minimum and median annual maximum discharge, which amounted to 1.06 m^3 s^{-1} and 3.50 m^3 s^{-1}, respectively. Optimal calibration results were obtained by a ratio of 1 between the frequency of observed and simulated peak discharges.

Second, we calibrated the sheet erosion estimates obtained from the MMF module. The calibration of the sheet erosion rates was performed per land use class and compared to the plot-scale soil loss data for the Mediterranean region obtained from Maetens et al. (2012b). We first calibrated the model parameters related to soil erodibility (K and DR) in the area covered by tree crops. We focussed on tree crops because we assume that their groundcover is negligible due to frequent ploughing. Next, we calibrated the soil erosion rates for the three other land use classes, i.e. forest, herbaceous crops and shrubland, using land use specific model parameters, such as groundcover, stem diameter and stem density. Optimal calibration results were obtained when the difference between the literature sheet erosion rates and the average simulated sheet erosion per land use class was smaller than 1%.

Finally, we calibrated the morphodynamics module using sediment yield data obtained from check dams in the Rogativa subcatchment (Boix-Fayos et al., 2007). The check dams are located on the hillslopes and in the main channel, hence, we divided the sediment yield dataset into two parts to account for model differences between the hillslopes and channels. On the hillslope, we focused on 17 non-silted check dams, which are thought to give the most reliable estimate of sediment yield. Unfortunately, all check dams in the main channel were silted, hence, for the channels we used all 6 silted check dams. The calibration of the morphodynamics module focused on two model parameters, i.e. the rill and channel bed thickness, which were used to, respectively, calibrate the sediment yield in the 17 check dams located on the hillslopes and in the 6 check dams located in the channels. Optimal calibration results were obtained by minimizing the root-mean-square error (RMSE).

4. Results

4.1. Model calibration

A similar annual maximum discharge distribution was obtained between the observed and simulated model run with optimal model parameters (Fig. 3a). The similarity between the two distributions is highlighted by comparable values for the maximum peak discharges, while the median peak discharges are slightly lower as simulated by the SPHY-MMF model. The Wilcox-test shows that no significant differences exist between the two distributions (p= 0.31). Despite differences in the time series, the frequency of peak discharge occurrence also shows similar results between observations and simulations (Fig. 3b). Comparable results are obtained for the occurrence of peak discharges larger than the observed minimum annual maximum discharge, with 142 occurrences from the observation dataset and 136 from the simulated model run. The occurrence of peak discharges higher than the median annual maximum discharge is somewhat overestimated, with 16 occurrences from the observation dataset and 33 from the simulated model run.

Sheet erosion for tree crops was optimized using the soil erodibility model parameters K_i and DR_i. We multiplied the values obtained by Quansah (1982) with 2.8 to obtain optimal model performance. For cereals we obtained optimal model performance by calibrating the

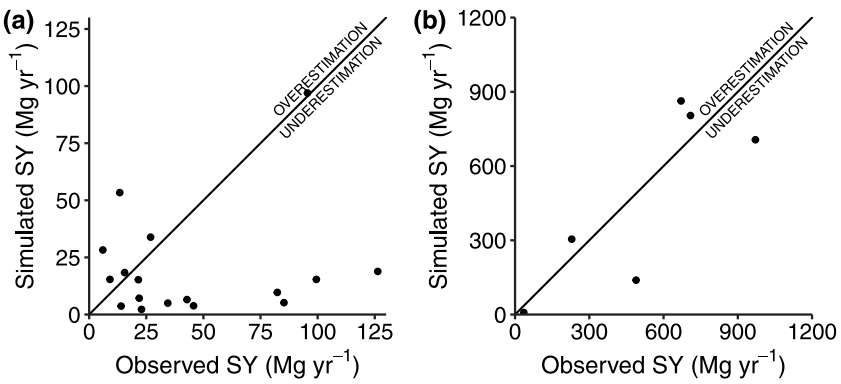

Fig. 4. Sediment yield (ton yr^{-1}) obtained at the check dams, with the observed SY on the horizontal axis and the simulated SY on the vertical axis: (a) the results for the non-silted check dams on the hillslopes and (b) the results for the silted check dams in the channels.

Table 2
Optimized values of the land use-specific model parameters of the MMF soil erosion model.

Parameter	Tree crops	Cereals	Forest	Shrubland
Plant height (m)	2	0.75	10	0.5
Manning's coefficient (s m$^{-1/3}$)	n/a	n/a	0.2	0.1
Stem density *NV* (stems m^{-1})	n/a	133	n/a	n/a
Stem diameter *D* (m)	n/a	0.017	n/a	n/a
Ground cover *GC* (–)	<0.01	0.0385	0.621	0.44

stem density and stem diameter (Table 2). For forest and shrubland we obtained Manning's coefficient values from Chow (1959) and used the ground cover for model calibration.

The calibration of the morphodynamics module resulted in a RMSE of 46.8 ton yr^{-1} (PBIAS −55.6%) for the check dams located on the hillslopes and 202.2 ton yr^{-1} (PBIAS −9.0%) for those located in the channels (Fig. 4), based on the optimum dimensionless rill bed thickness value of 0.0055 and channel bed thickness value of 0.0005. Sediment yield is underestimated in most check dams located on the hillslopes. The calibration results of the sediment yield in the check dams located in the channels are all positioned around the 1:1 line, suggesting a better fit.

4.2. Impact of land use change and check dam construction

The model was applied to a case study in the Rogativa subcatchment, which focusses on the reforestation and check dam construction that occurred between 1956 and 2016 (Fig. 2c). Sheet erosion contributed most to the total sediment yield in 1956 (Fig. 5). However, most of the sheet erosion (around 80% in both scenarios) is deposited in the rills, before arriving to the channel. Rill deposition occurs often in the area with higher rates of sheet erosion, which suggests that sediment eroded by sheet erosion is often deposited close to its origin. Channel deposition is negligible. About 65% of the total sediment yield at the catchment outlet originates from the hillslopes (i.e. net sheet and rill erosion), while the remainder originates from the channels.

Sheet erosion decreased with 52.3% between 1956 and 2016 (Fig. 5), which is mostly attributed to reforestation. Contrastingly, rill erosion increased with 16.0%. In 2016, the contribution from the hillslopes was similar to 1956, i.e. about 59.0%. Channel erosion slightly increased by 3.0%. Check dam construction led to a dramatic decrease in sediment yield at the outlet of 77.0%. The check dams trapped 74.8% of the total eroded sediment originating from the hillslopes and channels.

4.3. Impact of climate change

Similar to the results in the Rogativa subcatchment, sheet erosion contributed most to the total sediment yield in the Taibilla catchment in the reference scenario (1991–2020) (Fig. 6). In the Taibilla catchment, 83.6% of the sheet erosion is deposited in the rills and does not reach the channels. The hillslope contribution to the total sediment yield (i.e. net sheet and rill erosion) is similar to the Rogativa subcatchment, amounting to 59.9% of the total sediment yield. The remaining 40.1% originates from the channels. The total sediment yield at the Taibilla reservoir amounts to 16.3 Gg yr^{-1}.

All erosion sources are projected to increase in the +1.5 °C scenario, ultimately leading to an increase in sediment yield of 9.6%. Rill and channel erosion are projected to increase with 19.1% and 12.1%, respectively. Rill deposition is projected to increase with about the same rate as sheet erosion (~5%) and in most cases rill deposition increases on locations where sheet erosion increases, as well (Figure S2). Channel erosion is projected to increase most in the western part of the catchment and in the Rogativa subcatchment.

In the +3.0 °C scenario, sheet and channel erosion are projected to decrease with 10.0% and 26.2%, respectively. Rill erosion is projected to slightly increase with respect to the reference scenario (+2.0%). This will ultimately lead to a decrease in sediment yield at the outlet of 16.1%. Decrease of channel erosion is projected to occur in the majority of the tributaries of the main channel, such as in the Rogativa subcatchment (Figure S2). While the channel contribution to the total sediment yield remains the same for the +1.5 °C scenario (40.6%), the decrease in channel erosion in the +3.0 °C scenario causes the channel contribution to decrease to 33.9%.

5. Discussion

5.1. Model development

Here we present an upgrade to the SPHY-MMF model, which now simulates processes related to channel hydraulics and morphodynamics. The channel hydraulics module is based on a travel time algorithm, which is an approach that has been implemented in other soil erosion models with a daily time step, such as WEPP (Nearing et al., 1989) and INCA-Sed (Lazar et al., 2010). Our implementation of the travel time algorithm can obtain reliable catchment-scale discharge and flow velocity estimates through an iterative process. The number of iterative steps needed per daily time step depends on the spatial differences in runoff between two subsequent time steps, where more steps are needed in case of large spatial differences. This iterative process is in most cases limited to just a single step (around 90% of the time), but can reach up to 15 steps, for instance when a dry period is followed by a rainy day. The improved channel hydraulics module allows to generate flow velocity and water depth in each cell. These data are required to estimate sediment transport rates, as in the current application, but can also be used to study other channel processes, for instance to couple the hydraulics module to habitat suitability models (Yi et al., 2017). This makes the new model more versatile to be applied in

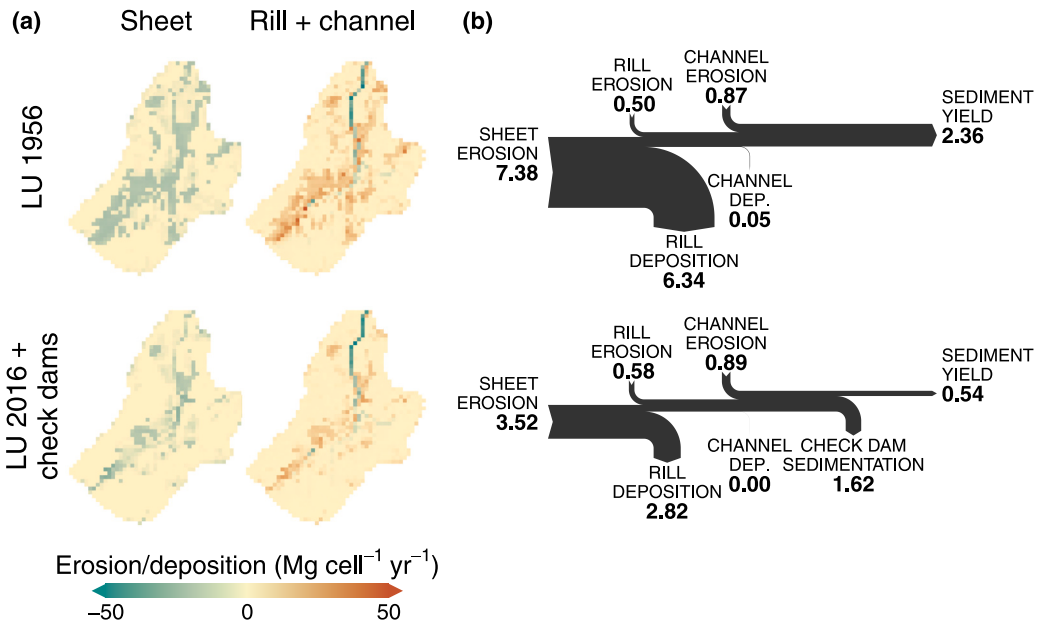

Fig. 5. Model results for the Rogativa subcatchment, for the 1956 land use scenario (upper row) and the 2016 land use scenario, including check dam construction (lower row). (a) Sheet erosion and rill and channel change (Mg cell^{-1} yr^{-1}), where blue colours indicate erosion and red colours deposition. (b) The sediment balance (Gg yr^{-1}) for all the considered processes.

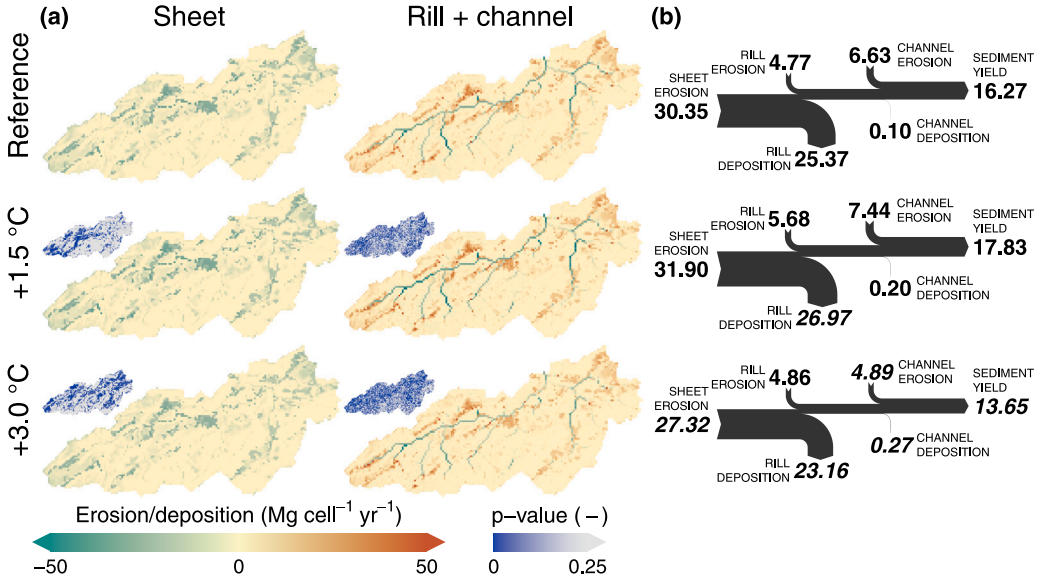

Fig. 6. Model results for the Taibilla catchment, for the reference (1991–2020) scenario (upper row), the +1.5 °C scenario (middle row) and the +3.0 °C scenario (lower row). (a) Sheet erosion and rill and channel change (Mg cell^{-1} yr^{-1}), where blue colours indicate erosion and red colours deposition. (b) The sediment balance (Gg yr^{-1}) for all the considered processes. Values in italic indicate significant changes ($p < 0.05$) with respect to the reference scenario.

different environmental contexts, such as to study large-scale river hydraulics, flood impacts, channel morphodynamics and impacts on aquatic ecology.

Currently, the revision of the sediment transport module and the implementation of a morphodynamics module allows the model to make assessments of the catchment-scale sediment balance, including sheet erosion and erosion and deposition in rills and channels. The separation between sediment transport in rills and channels, here using the Govers (1990) and Yalin (1963) equations, respectively, has been adopted in other process-based soil erosion models, e.g SHETRAN (Lukey et al., 1995) and LISEM (De Roo et al., 1996). This separation between the two model domains is applied because of the inherit differences in sediment transport processes between rills and channels. For instance, rills usually have steeper slopes, resulting in laminar flows, while the bed material is often more cohesive, affecting sediment transport conditions (Hessel and Jetten, 2007). Channel beds often consist of coarser material, for which different sediment transport equations are developed, and sediment may be transported in suspension, while sediment transport in rills is mostly limited to bedload transport (Hessel and Jetten, 2007). The morphodynamics module is based on sediment storage, which is the sum of the locally generated sheet erosion and the available sediment in the rill/channel bed. This approach is similar to those applied in other models, e.g. INCA-Sed (Lazar et al., 2010), SHETRAN (Lukey et al., 1995) and TETIS (Bussi et al., 2013). While these other models incorporate similar processes, the SPHY-MMF model includes less model parameters, which improves the applicability of the model to larger scales and data-scarce areas. For instance, the channel hydraulics module is mainly controlled by the Manning's roughness

coefficient, for which we adopted literature values for the rills, channels and floodplain (Chow, 1959). Similarly, the morphodynamics module is mainly controlled by the thickness of the available bed material, differentiated for rills and channels. Therefore, the SPHY-MMF model may be a step forward with respect to similar models in terms of reduced model complexity and improved model applicability.

Similar to the previously mentioned models, the SPHY-MMF model requires channel dimensions and bed material estimates for the entire channel network. While all other input data, including climate data, soil characteristics, land use maps, were obtained from large open-source datasets, channel characteristics are often not available for large-scale model applications. The use of aerial photo interpretation combined with high resolution LiDAR data and a limited number of field control points, as was used in this study, might provide a solution to obtain information on channel dimensions. However, our model application was performed in a relatively small catchment, which facilitates the use of this method to obtain channel characteristics. To obtain reliable channel characteristics in larger catchments (i.e. >10,000 km^2), for which the model was designed, may be more problematic. This may be overcome by obtaining the channel characteristics through multiple regression models (e.g. Bieger et al., 2016). However, such models most likely get more reliable results when calibrated with locally obtained data, which still requires data acquisition through fieldwork or from remote sensing data. Hence, obtaining data on channel dimensions remains challenging for the application to larger spatial scales, when channel characteristics are unknown or have to be estimated based on proxies.

5.2. Model application

The model was applied to two case studies. First, the model was applied to the Rogativa subcatchment, with a comparison between the catchment configuration for 1956 and 2016, in which period the subcatchment was subject to reforestation and check dam construction. The case study showed a decrease in sheet erosion from 1956 to 2016 (Fig. 5), which can be explained by the natural recovery of the forest vegetation and reforestation programs that occurred between 1956 and 2016 (Fig. 2c), resulting in a significant increase in canopy and ground cover in the catchment. The decrease in sediment supply from the hillslopes resulted in an increase in rill and channel erosion, i.e. an increase in concentrated flow erosion following reforestation. Channel erosion increased less than rill erosion, which could be related to the cascading effect of the rills flowing into the channels, where the sediment input from the rills into the channels was already somewhat near the transport capacity of the channels. In 2016, a large proportion (74.8%) of the sediment originating from the hillslopes and channels is deposited behind check dams that were built at the end of the 1970s. Our results show that check dam sedimentation contributed most to the 77.0% decrease in sediment yield with respect to 1956. However, several large check dams trapped almost as much sediment as their constructed capacity during the 30 year simulation period (Fig. 7), in which case their trapping efficiency would be strongly reduced.

Boix-Fayos et al. (2007) studied the impact of land use change and check dam construction on channel morphodynamics in the Rogativa subcatchment, which was based on two different sources, i.e. historical aerial photos and field data. They showed that channel erosion occurred in the period after reforestation and check dam construction, including channel incision, channel narrowing, bank erosion and armouring of the channel bed. Boix-Fayos et al. (2007) also suggest a transition from a situation characterized by a wide braided channel with active, dynamic channel bars before reforestation and check dam construction to a situation characterized by a rather static single thread channel pattern, with occasional bank erosion and channel incision. Our results show that the decreased sediment input from the hillslopes as a response to reforestation and the construction of check dams outside the main channel did provoke a slight increase in channel erosion.

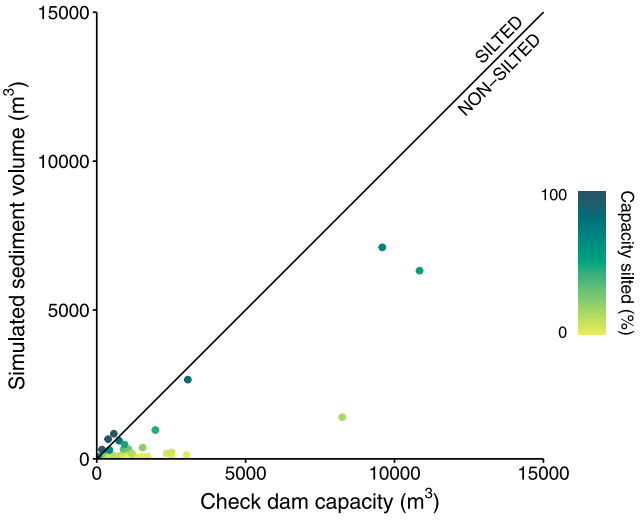

Fig. 7. Comparison between the initial check dam capacity (m^3) and simulated sediment volume (m^3) over the 30-year simulation period (1991–2020), considering check dams and the land use map of 2016 in the Rogativa subcatchment.

The two scenarios in the current study (1956 and 2016) may represent two situations of (quasi) morphological equilibrium, where it is likely that in the transition period (i.e. the first 10–15 years after reforestation and check dam construction) most channel erosion occurred, which may be due to two processes not accounted for by the model. First of all, the channel erosion may be due to vegetation encroachment on the floodplains, as observed by Boix-Fayos et al. (2007) and Halifa-Marín et al. (2019), causing channel confinement and incision. And second, while check dam construction on the hillslopes and reforestation may have led to a prompt decrease in sediment input from the hillslopes, the impact of reforestation on the hydrological response of the catchment may still have been limited, as described by some geomorphological models (Simon and Darby, 2002). This might have resulted in a situation with lower hillslope sediment input, but with still relatively high runoff from the hillslopes and high flow velocities in the channels, which may have contributed to the observed channel erosion. The relatively quick adjustment of the soil erosion dynamics and slower response to the catchment hydrology has been observed in other studies (e.g. Calvo-Cases et al., 2003; Martínez-Mena et al., 2020), which could be simulated by the SPHY-MMF model by gradually adjusting the vegetation cover and soil organic carbon content in the soil, but is out of the scope of the current study.

In the second case study in the Taibilla catchment, we assessed the climate change impact on the catchment-scale sediment balance. In the reference scenario (1991–2020), the total sediment yield at the Taibilla reservoir was estimated to be 16.3 Gg yr^{-1}, which is an underestimation of the measured reservoir sediment yield of 130 Gg yr^{-1} (Avendaño-Salas et al., 1997). The reason for this difference might be related to the calibration of the morphodynamics module. The calibration of the channel morphodynamics was based on only 6 check dams in the Rogativa subcatchment (Fig. 4b), which might give a biased estimate of sediment yield. On top of that, these 6 check dams turned out to be fully silted when the volume of trapped sediment was measured by Boix-Fayos et al. (2007). Therefore, it is likely that the obtained measured sediment yield estimates are an underestimation of the real sediment yield, which might have led to an underestimation of channel erosion and, subsequently, sediment yield at the reservoir. At the same time, the calibration of the sediment yield in the check dams located on the hillslopes also resulted in an underestimation of sediment yield (Fig. 4). Moreover, the scenario results (Figs. 5 and 6) show that the majority of the sheet erosion is deposited in the rills. Both the underestimation of the check dam sediment yield and

the high deposition rate in the rills might suggest an underestimation of the transport capacity in the rills. We implemented the (Govers, 1990) sediment transport equation, which has been implemented in other soil erosion models, such as EUROSEM (Morgan et al., 1998) and LISEM (De Roo et al., 1996). Alternatives for the (Govers, 1990) equation are the equations by Abrahams et al. (2001) and Ali et al. (2013), which were also developed for rills. Future research is needed to test these equations in SPHY-MMF and assess their applicability in the study area and other environments. While this study provides an importance advance regarding the differentiation between hillslope and channel erosion processes, further research is required to identify which transport equations are most appropriate in the continuum from rills, to gullies and channels.

Both case studies show that channel erosion has a significant contribution (35%–40%) to the catchment-scale sediment yield, which is in the range of observed channel contribution estimates made by Hamlett et al. (1983) (25%–50%), Trimble (1997) (71%), Wilson et al. (2008) (avg. 68%), and Wang et al. (2013) (avg. 40%). While these observations were made under different climatic and geographic conditions, the catchment size considered in these studies are of the same order of magnitude as used in the current study. This might indicate that channels may contribute significantly to the total sediment balance in small to medium sized catchments.

The land use and check dam construction scenario in the Rogativa subcatchment showed that the check dams trapped about 75% of the sediment originating from the hillslopes and the channels (Fig. 5). Hence, the check dams were effective conservation measure to reduce the sediment yield, especially those constructed in the main channel. However, the majority of the check dams were silted within 25 years of their construction (Boix-Fayos et al., 2007), where it is likely that the trapping efficiency of the silted check dams decreased significantly. Simulations also showed that several check dams trapped more sediment than their initial capacity in the 2016 scenario (Fig. 7). Hence, other conservation measures need to be considered to reduce sediment yield more sustainably (Boix-Fayos et al., 2020). The majority of the sheet erosion is deposited in the rills (i.e. 85.9% in the case of the Rogativa in 1956; Fig. 5b), therefore, reducing sheet erosion might not be the most effective way to reduce sediment yield in this study area. About 60% of the sediment yield at the outlet is supplied from the hillslopes, with the largest contribution from rill erosion. Therefore, sediment supply towards the channels might be reduced by applying conservation measures in the sediment flow paths on the hillslopes with the highest contribution, for instance by implementing vegetated buffer strips (Gumiere et al., 2011). Assuming static hydrological conditions, a reduction of the hillslope sediment input towards the channels might cause an increase of channel erosion. This increase in channel erosion can be counteracted by applying river restoration in the channels, such as floodplain lowering and widening and introduction of riparian vegetation (Eekhout et al., 2015), which will reduce the flow velocity and, subsequently, the transport capacity in the channels. Such Nature-based Solutions (Cohen-Shacham et al., 2016) might be more effective and are lower in maintenance than grey infrastructure, such as check dams (Boix-Fayos et al., 2020). Nevertheless, evaluation of their effectiveness under current and future climate conditions with more extreme precipitation still requires more research.

5.3. Climate change impacts on channel morphodynamics

The impact of climate change on channel morphodynamics has been considered before, which in most cases included the application of a 1D- or 2D-morphodynamic model to study areas consisting of river reaches (e.g. Verhaar et al., 2010; Guerrero et al., 2013; Shrestha et al., 2020; Crosato et al., 2022), rather than the entire stream network as applied in the current study. While there are exceptions (e.g. Guerrero et al., 2013; Lee et al., 2021), most of these studies assume sediment capacity as boundary condition for upstream sediment input (e.g. Verhaar et al., 2010; Crosato et al., 2022). Our application of the model in the Rogativa subcatchment and Taibilla catchment show that rill deposition occurs, which suggests that rills are capacity limited. On the other hand, channel deposition is negligible, which suggest that the channels are supply limited. Hence, the assumption of transport capacity at the upstream boundary, like in the before mentioned studies, would have resulted in an underestimation of channel erosion in our case, because of the supply-limited conditions in the channels. Such assumptions are not needed when coupling a soil erosion model to a channel morphodynamics model, as presented in the current study.

When a similar approach was used in a climate change impact study, then in most cases the SWAT model (Arnold et al., 2012) was used to assess the combined impact of soil erosion and channel morphodynamics (e.g. Shrestha et al., 2013; Mukundan et al., 2013; Praskievicz, 2015; Shrestha and Wang, 2018; Sharafati et al., 2020). Several of these studies suggest that the channel contribution is likely to increase under climate change, because of the increase in runoff and peak discharges, which will increase channel erosion (Mukundan et al., 2013; Praskievicz, 2015; Shrestha and Wang, 2018). Similar conclusions were made by Neverman et al. (2023), who suggest an increase in mass movements and bank erosion in New Zealand under climate change. An increase in channel morphodynamic changes is also shown by studies that apply 1D- or 2D-morphodynamic models (e.g. Praskievicz, 2015; Morianou et al., 2018; Shrestha et al., 2020; Lee et al., 2021), which also relate the increase in channel morphodynamics to increasing peak discharges as a response to an increase in extreme rainfall events. Our results show similarities to these previous studies, especially regarding the +1.5 °C scenario, where an increase in channel erosion is projected as a response to an increase in annual and extreme precipitation. However, in the +3.0 °C scenario, the model projects a decrease in channel erosion, as a response to a strong decrease in annual precipitation and a lower increase in extreme precipitation compared to the +1.5 °C scenario. This suggests that an increase in extreme precipitation not automatically leads to an increase in channel erosion. Moreover, changes in hillslope erosion (i.e. sheet and rill erosion) affect channel morphodynamics in different ways considering differences in climate signal between climate change scenarios. More research is needed that focus on differences in climate signals and their impact on the catchment-scale sediment balance.

6. Conclusions

Here we present an upgrade to the coupled hydrological-soil erosion model SPHY-MMF, with the implementation of channel hydraulics and morphodynamics modules to the existing model. The model is able to give an estimate of the catchment-scale sediment balance and sediment yield, considering sheet erosion, and erosion and deposition in rills and channels. Furthermore, the model simulates check dam and reservoir sedimentation. The model was applied to a Mediterranean catchment in southeast Spain. Calibration of the morphodynamics module was based on measured sediment yield data, which gave satisfactory results for the check dams located in the main channels, but an underestimation for those located in smaller tributaries. A historical land use change scenario was performed in a subcatchment that has been subject to reforestation and check dam construction. Our results show that channel erosion contributes about 35%–40% of the sediment yield at the catchment outlet, highlighting the importance of accounting for channel erosion in catchment-scale sediment budget estimations. Land use change and check dam construction caused a decrease of sediment yield, which is partly due to the decrease of sheet erosion as a response to reforestation, but mostly due to the sedimentation behind check dams.

In comparison to many previous studies on the impact of climate change on sediment yield, the current model is able to give a more complete estimate of the sediment balance under future climate change. The results show that rill erosion is projected to increase in both climate

change scenarios, which is most likely related to the projected increase in extreme precipitation. However, other erosional processes (i.e. sheet and channel) are projected to decrease or increase, depending on the future scenario. This difference in response is likely related to the projected change in annual precipitation. Ultimately, this leads to a significant increase of sediment yield in case of the combined increase in annual precipitation and extreme precipitation, and a decrease in sediment yield for the scenario where annual precipitation is projected to decrease. From this we conclude that these different erosional and depositional processes and their interactions should be considered when studying the future change in the catchment-scale sediment yield. This will also allow policy makers to plan conservation measures more efficiently, by applying measures close to the sources with the highest contribution to the catchment-scale sediment yield, accounting for possible interactions with other erosion or deposition processes within the catchment.

Software availability

This manuscript presents modifications to the SPHY-MMF model, which was developed by Joris Eekhout (joriseekhout@gmail.com) and Joris de Vente, in collaboration with FutureWater (info@futurewater.nl). The SPHY-MMF model is written in the Python programming language and makes use of the PCRaster modelling framework (Karssenberg et al., 2010). The exact version of the model used to produce the results used in this paper is archived and freely available on Zenodo (Eekhout and de Vente, 2023).

Declaration of competing interest

The authors declare that they have no known competing financial interests or personal relationships that could have appeared to influence the work reported in this paper.

Acknowledgements

We acknowledge funding from the Spanish Ministry of Science and Innovation and 'Agencia Estatal de Investigación' through the XTREME (PID2019-109381RB-I00/AEI/10.13039/501100011033) and RESTORE-NBS projects (202040E030), the European Union (NextGenerationEU; PRTR-C17.I1), and Fundación Séneca and the Comunidad Autónoma Región de Murcia (CARM) through the AGROALNEXT programme. Joris Eekhout was supported by a Juan de la Cierva - Incorporación fellowship (IJC2020-044636-I). The authors thank AEMET for the data provided to carry out this work (AEMET's 5 km rainfall grid).

Appendix A. Supplementary data

Supplementary material related to this article can be found online at https://doi.org/10.1016/j.envsoft.2023.105890.

References

Abrahams, A.D., Li, G., Krishnan, C., Atkinson, J.F., 2001. A sediment transport equation for interrill overland flow on rough surfaces. Earth Surf. Process. Landf. 26, 1443–1459. http://dx.doi.org/10.1002/esp.286.

Aksoy, H., Kavvas, M.L., 2005. A review of hillslope and watershed scale erosion and sediment transport models. Catena 64, 247–271. http://dx.doi.org/10.1016/j.catena.2005.08.008.

Ali, M., Seeger, M., Sterk, G., Moore, D., 2013. A unit stream power based sediment transport function for overland flow. CATENA 101, 197–204. http://dx.doi.org/10.1016/j.catena.2012.09.006.

Amundson, R., Berhe, A.A., Hopmans, J.W., Olson, C., Sztein, A.E., Sparks, D.L., 2015. Soil and human security in the 21st century. Science 348, 1261071. http://dx.doi.org/10.1126/science.1261071.

Arnold, J.G., Moriasi, D.N., Gassman, P.W., Abbaspour, K.C., White, M.J., Srinivasan, R., Santhi, C., Harmel, R.D., Griensven, a.V., VanLiew, M.W., Kannan, N., Jha, M.K., 2012. Swat: Model use, calibration, and validation. Asabe 55, 1491–1508.

Avendaño-Salas, C., Sanz-Montero, E., Cobo-Rayán, R., Gómez-Montaña, J.L., 1997. Sediment yield at Spanish Reservoirs and its relationship with the Drainage Basin Area. In: ICOLD, Proceedings of the 19th International Symposium on Large Dams. Florence, pp. 863–874.

Batista, P.V.G., Fiener, P., Scheper, S., Alewell, C., 2022. A conceptual-model-based sediment connectivity assessment for patchy agricultural catchments. Hydrol. Earth Syst. Sci. 26, 3753–3770. http://dx.doi.org/10.5194/hess-26-3753-2022.

Ben Slimane, A., Raclot, D., Evrard, O., Sanaa, M., Lefevre, I., Le Bissonnais, Y., 2016. Relative contribution of rill/interrill and gully/channel erosion to small reservoir siltation in Mediterranean environments. Land Degrad. Dev. 27, 785–797. http://dx.doi.org/10.1002/ldr.2387.

Bieger, K., Rathjens, H., Arnold, J.G., Chaubey, I., Allen, P.M., 2016. Development and comparison of multiple regression models to predict bankfull channel dimensions for use in hydrologic models. JAWRA J. Am. Water Resour. Assoc. 52, 1385–1400. http://dx.doi.org/10.1111/1752-1688.12460.

Bizzi, S., Tangi, M., Schmitt, R.J.P., Pitlick, J., Piégay, H., Castelletti, A.F., 2021. Sediment transport at the network scale and its link to channel morphology in the braided Vjosa River system. Earth Surf. Process. Landf. 1–17. http://dx.doi.org/10.1002/esp.5225.

Boix-Fayos, C., Barberá, G.G., López-Bermúdez, F., Castillo, V.M., 2007. Effects of check dams, reforestation and land-use changes on river channel morphology: Case study of the Rogativa catchment (Murcia, Spain). Geomorphology 91, 103–123. http://dx.doi.org/10.1016/j.geomorph.2007.02.003.

Boix-Fayos, C., Boerboom, L.G., Janssen, R., Martínez-Mena, M., Almagro, M., Pérez-Cutillas, P., Eekhout, J.P., Castillo, V., de Vente, J., 2020. Mountain ecosystem services affected by land use changes and hydrological control works in Mediterranean catchments. Ecosyst. Serv. 44, 101136. http://dx.doi.org/10.1016/j.ecoser.2020.101136.

Boix-Fayos, C., de Vente, J., Martínez-Mena, M., Barberá, G.G., Castillo, V., 2008. The impact of land use change and check-dams on catchment sediment yield. Hydrol. Process. 22, 4922–4935. http://dx.doi.org/10.1002/hyp.7115.

Brown, C.B., 1943. Discussion of sedimentation in reservoirs. Proc. Am. Soc. Civ. Eng. 69, 1493–1500.

Bussi, G., Rodríguez-Lloveras, X., Francés, F., Benito, G., Sánchez-Moya, Y., Sopeña, A., 2013. Sediment yield model implementation based on check dam infill stratigraphy in a semiarid Mediterranean catchment. Hydrol. Earth Syst. Sci. 17, 3339–3354. http://dx.doi.org/10.5194/hess-17-3339-2013.

Calvo-Cases, A., Boix-Fayos, C., Imeson, A., 2003. Runoff generation, sediment movement and soil water behaviour on calcareous (limestone) slopes of some Mediterranean environments in southeast Spain. Geomorphology 50, 269–291. http://dx.doi.org/10.1016/S0169-555X(02)00218-0.

Camporeale, C., Perona, P., Porporato, A., Ridolfi, L., 2007. Hierarchy of models for meandering rivers and related morphodynamic processes: Hierarchy of models for Meandering Rivers. Rev. Geophys. 45, http://dx.doi.org/10.1029/2005RG000185.

Chow, V.T., 1959. Open-channel Hydraulics. McGraw-Hill Book Company, New York, US, ISBN: 978-1932846188.

Cohen-Shacham, E., Walters, G., Janzen, C., Maginnis, S., 2016. Nature-Based Solutions To Address Global Societal Challenges. IUCN, Gland, Switzerland, http://dx.doi.org/10.2305/iucn.ch.2016.13.en.

Crosato, A., Grissetti-Vázquez, A., Bregoli, F., Franca, M., 2022. Adaptation of river channels to a wetter or drier climate: Insights from the Lower Pilcomayo River, South America. J. Hydrol. 612, 128254. http://dx.doi.org/10.1016/j.jhydrol.2022.128254.

De Roo, A.P.J., Wesseling, C.G., Ritsema, C.J., 1996. LISEM: A single-event physically based hydrological and soil erosion model for drainage basins I: Theory, input and output. Hydrol. Process. 10, 1107–1117. http://dx.doi.org/10.1002/(SICI)1099-1085(199608)10:8<1107::AID-HYP415>3.3.CO;2-W.

de Vente, J., Poesen, J., Arabkhedri, M., Verstraeten, G., 2007. The sediment delivery problem revisited. Prog. Phys. Geogr. 31, 155–178. http://dx.doi.org/10.1177/0309133307076485.

de Vente, J., Poesen, J., Verstraeten, G., 2005. The application of semi-quantitative methods and reservoir sedimentation rates for the prediction of basin sediment yield in Spain. J. Hydrol. 305, 63–86. http://dx.doi.org/10.1016/j.jhydrol.2004.08.030.

de Vente, J., Poesen, J., Verstraeten, G., Govers, G., Vanmaercke, M., Van Rompaey, A., Arabkhedri, M., Boix-Fayos, C., 2013. Predicting soil erosion and sediment yield at regional scales: Where do we stand? Earth-Sci. Rev. 127, 16–29. http://dx.doi.org/10.1016/j.earscirev.2013.08.014.

de Vente, J., Poesen, J., Verstraeten, G., Van Rompaey, A., Govers, G., 2008. Spatially distributed modelling of soil erosion and sediment yield at regional scales in Spain. Glob. Planet. Change 60, 393–415. http://dx.doi.org/10.1016/j.gloplacha.2007.05.002.

Didan, K., 2015. MOD13Q1 MODIS/Terra vegetation indices 16-Day L3 Global 250 m SIN grid V006. http://dx.doi.org/10.5067/modis/mod13q1.006.

Eekhout, J.P.C., Boix-Fayos, C., Pérez-Cutillas, P., de Vente, J., 2020. The impact of reservoir construction and changes in land use and climate on ecosystem services in a large Mediterranean catchment. J. Hydrol. 590, 125208. http://dx.doi.org/10.1016/j.jhydrol.2020.125208.

Eekhout, J.P.C., de Vente, J., 2019a. Assessing the effectiveness of Sustainable Land Management for large-scale climate change adaptation. Sci. Total Environ. 654, 85–93. http://dx.doi.org/10.1016/j.scitotenv.2018.10.350.

Eekhout, J.P.C., de Vente, J., 2019b. The implications of bias correction methods and climate model ensembles on soil erosion projections under climate change. Earth Surf. Process. Landf. 44, 1137–1147. http://dx.doi.org/10.1002/esp.4563.
Eekhout, J.P.C., de Vente, J., 2020. How soil erosion model conceptualization affects soil loss projections under climate change. Prog. Phys. Geogr. Earth Environ. 44, 212–232. http://dx.doi.org/10.1177/0309133319871937.
Eekhout, J.P.C., de Vente, J., 2022. Global impact of climate change on soil erosion and potential for adaptation through soil conservation. Earth-Sci. Rev. 226, 103921. http://dx.doi.org/10.1016/j.earscirev.2022.103921.
Eekhout, J., de Vente, J., 2023. SPHY-MMF - Coupled Hydrology-Hillslope and Channel Erosion Model. Zenodo, http://dx.doi.org/10.5281/ZENODO.7997412.
Eekhout, J.P.C., Hoitink, A.J.F., de Brouwer, J.H.F., Verdonschot, P.F.M., 2015. Morphological assessment of reconstructed lowland streams in the Netherlands. Adv. Water Resour. 81, 161–171. http://dx.doi.org/10.1016/j.advwatres.2014.10.008.
Eekhout, J.P.C., Hoitink, A.J.F., Mosselman, E., 2013. Field experiment on alternate bar development in a straight sand-bed stream. Water Resour. Res. 49, 8357–8369. http://dx.doi.org/10.1002/2013WR014259.
Eekhout, J.P.C., Hunink, J.E., Terink, W., de Vente, J., 2018a. Why increased extreme precipitation under climate change negatively affects water security. Hydrol. Earth Syst. Sci. 22, 5935–5946. http://dx.doi.org/10.5194/hess-22-5935-2018.
Eekhout, J.P.C., Terink, W., de Vente, J., 2018b. Assessing the large-scale impacts of environmental change using a coupled hydrology and soil erosion model. Earth Surf. Dyn. 6, 687–703. http://dx.doi.org/10.5194/esurf-6-687-2018.
Govers, G., 1990. Empirical relationships for the transport capacity of overland flow. In: Erosion, Transport and Deposition Processes, Vol. 189. IAHS Publ., pp. 45–63.
Govers, G., 2011. Misapplications and Misconceptions of erosion models. In: Morgan, R.P.C., Nearing, M.A. (Eds.), Handbook of Erosion Modelling. John Wiley & Sons, Ltd, Chichester, UK, pp. 117–134. http://dx.doi.org/10.1002/9781444328455.ch7.
Govers, G., Giménez, R., Van Oost, K., 2007. Rill erosion: Exploring the relationship between experiments, modelling and field observations. Earth-Sci. Rev. 84, 87–102. http://dx.doi.org/10.1016/j.earscirev.2007.06.001.
Guerrero, M., Nones, M., Saurral, R., Montroull, N., Szupiany, R.N., 2013. Parana River morphodynamics in the context of climate change. Int. J. River Basin Manag. 11, 423–437. http://dx.doi.org/10.1080/15715124.2013.826234.
Gumiere, S.J., Le Bissonnais, Y., Raclot, D., Cheviron, B., 2011. Vegetated filter effects on sedimentological connectivity of agricultural catchments in erosion modelling: A review. Earth Surf. Process. Landf. 36, 3–19. http://dx.doi.org/10.1002/esp.2042.
Halifa-Marín, A., Pérez-Cutillas, P., Almagro, M., Martínez-Mena, M., Boix-Fayos, C., 2019. Dinámica geomorfológica fluvial y cambios de usos del suelo: Impacto en los reservorios de carbono de suelos y sedimentos. Bosque (Valdivia) 40, 3–16. http://dx.doi.org/10.4067/S0717-92002019000100003.
Hamlett, J.M., Baker, J.L., Johnson, H.P., 1983. Channel morphology changes and sediment yield for a small agricultural watershed in Iowa. Trans. ASAE 26, 1390–1396. http://dx.doi.org/10.13031/2013.34138.
Hargreaves, G.H., Samani, Z.A., 1985. Reference crop evapotranspiration from temperature. Appl. Eng. Agric. 1, 96–99.
Heber Green, W., Ampt, G.A., 1911. Studies on soil phyics. J. Agric. Sci. 4, 1–24. http://dx.doi.org/10.1017/S0021859600001441.
Hengl, T., Mendes de Jesus, J., Heuvelink, G.B.M., Ruiperez Gonzalez, M., Kilibarda, M., Blagotić, A., Shangguan, W., Wright, M.N., Geng, X., Bauer-Marschallinger, B., Guevara, M.A., Vargas, R., MacMillan, R.A., Batjes, N.H., Leenaars, J.G.B., Ribeiro, E., Wheeler, I., Mantel, S., Kempen, B., 2017. SoilGrids250m: Global gridded soil information based on machine learning. PLoS One 12, e0169748. http://dx.doi.org/10.1371/journal.pone.0169748.
Hessel, R., Jetten, V., 2007. Suitability of transport equations in modelling soil erosion for a small Loess Plateau catchment. Eng. Geol. 91, 56–71. http://dx.doi.org/10.1016/j.enggeo.2006.12.013.
Ikeda, S., Parker, G., Sawai, K., 1981. Bend theory of river meanders. Part 1. Linear development. J. Fluid Mech. 112, 363. http://dx.doi.org/10.1017/S0022112081000451.
Jacob, D., Petersen, J., Eggert, B., Alias, A., Christensen, O.B., Bouwer, L.M., Braun, A., Colette, A., Déqué, M., Georgievski, G., Georgopoulou, E., Gobiet, A., Menut, L., Nikulin, G., Haensler, A., Hempelmann, N., Jones, C., Keuler, K., Kovats, S., Kröner, N., Kotlarski, S., Kriegsmann, A., Martin, E., van Meijgaard, E., Moseley, C., Pfeifer, S., Preuschmann, S., Radermacher, C., Radtke, K., Rechid, D., Rounsevell, M., Samuelsson, P., Somot, S., Soussana, J.-F., Teichmann, C., Valentini, R., Vautard, R., Weber, B., Yiou, P., 2014. EURO-CORDEX: New high-resolution climate change projections for European impact research. Reg. Environ. Change 14, 563–578. http://dx.doi.org/10.1007/s10113-013-0499-2.
Jin, C.X., Römkens, J.M., Griffioen, F., 2000. Estimating manning's roughness coefficient for shallow overland flow in non-submerged vegetative filter strips. Trans. ASAE 43, 1459–1466.
Jodar-Abellan, A., Ruiz, M., Melgarejo, J., 2018. Evaluación del impacto del cambio climático sobre una cuenca hidrológica en régimen natural (SE, España) usando un modelo SWAT. Revista Mexicana Ciencias Geol. 35, 240–253. http://dx.doi.org/10.22201/cgeo.20072902e.2018.3.564.
Karssenberg, D., Schmitz, O., Salamon, P., de Jong, K., Bierkens, M.F., 2010. A software framework for construction of process-based stochastic spatio-temporal models and data assimilation. Environ. Model. Softw. 25, 489–502. http://dx.doi.org/10.1016/j.envsoft.2009.10.004.
Kirkby, M.J., Irvine, B.J., Jones, R.J.A., Govers, G., 2008. The PESERA coarse scale erosion model for Europe. I. - Model rationale and implementation. Eur. J. Soil Sci. 59, 1293–1306. http://dx.doi.org/10.1111/j.1365-2389.2008.01072.x.
Knighton, D., 1998. Fluvial Forms and Processes. Routledge, http://dx.doi.org/10.4324/9780203784662.
Knisel, W.G., 1980. Creams: A Field Scale Model for Chemicals, Runoff, and Erosion from Agricultural Management Systems. Number 26 in Conservation Research Report, United States Department of Agriculture.
Koch, A., McBratney, A., Adams, M., Field, D., Hill, R., Crawford, J., Minasny, B., Lal, R., Abbott, L., O'Donnell, A., Angers, D., Baldock, J., Barbier, E., Binkley, D., Parton, W., Wall, D.H., Bird, M., Bouma, J., Chenu, C., Flora, C.B., Goulding, K., Grunwald, S., Hempel, J., Jastrow, J., Lehmann, J., Lorenz, K., Morgan, C.L., Rice, C.W., Whitehead, D., Young, I., Zimmermann, M., 2013. Soil security: Solving the global soil crisis. Glob. Policy 4, 434–441. http://dx.doi.org/10.1111/1758-5899.12096.
Lagacherie, P., Álvaro-Fuentes, J., Annabi, M., Bernoux, M., Bouarfa, S., Douaoui, A., Grünberger, O., Hammani, A., Montanarella, L., Mrabet, R., Sabir, M., Raclot, D., 2018. Managing Mediterranean soil resources under global change: Expected trends and mitigation strategies. Reg. Environ. Change 18, 663–675. http://dx.doi.org/10.1007/s10113-017-1239-9.
Langendoen, E.J., Simon, A., 2008. Modeling the evolution of incised streams. II: Streambank erosion. J. Hydraul. Eng. 134, 905–915. http://dx.doi.org/10.1061/(ASCE)0733-9429(2008)134:7(905).
Lazar, A.N., Butterfield, D., Futter, M.N., Rankinen, K., Thouvenot-Korppoo, M., Jarritt, N., Lawrence, D.S., Wade, A.J., Whitehead, P.G., 2010. An assessment of the fine sediment dynamics in an upland river system: INCA-Sed modifications and implications for fisheries. Sci. Total Environ. 408, 2555–2566. http://dx.doi.org/10.1016/j.scitotenv.2010.02.030.
Lee, J.M., Ahn, J., Kim, Y.D., Kang, B., 2021. Effect of climate change on long-term river geometric variation in Andong Dam watershed, Korea. J. Water Clim. Chang. 12, 741–758. http://dx.doi.org/10.2166/wcc.2020.148.
Lotsari, E., Thorndycraft, V., Alho, P., 2015. Prospects and challenges of simulating river channel response to future climate change. Prog. Phys. Geogr. Earth Environ. 39, 483–513. http://dx.doi.org/10.1177/0309133315578944.
Lukey, B.T., Bathurst, J.C., Hiley, R.A., Ewen, J., 1995. SHETRAN Sediment Transport Component: Equations and Algorithms. Technical Report, University of Newcastle upon Tyne, Newcastle, United Kingdom.
Maetens, W., Poesen, J., Vanmaercke, M., 2012a. How effective are soil conservation techniques in reducing plot runoff and soil loss in Europe and the Mediterranean? Earth-Sci. Rev. 115, 21–36. http://dx.doi.org/10.1016/j.earscirev.2012.08.003.
Maetens, W., Vanmaercke, M., Poesen, J., Jankauskas, B., Jankauskiene, G., Ionita, I., 2012b. Effects of land use on annual runoff and soil loss in Europe and the Mediterranean: A meta-analysis of plot data. Prog. Phys. Geogr. 36, 599–653. http://dx.doi.org/10.1177/0309133312451303.
Martínez-Mena, M., Carrillo-López, E., Boix-Fayos, C., Almagro, M., García Franco, N., Díaz-Pereira, E., Montoya, I., De Vente, J., 2020. Long-term effectiveness of sustainable land management practices to control runoff, soil erosion, and nutrient loss and the role of rainfall intensity in Mediterranean rainfed agroecosystems. CATENA 187, 104352. http://dx.doi.org/10.1016/j.catena.2019.104352.
Ministerio de Fomento de España, 2015. Plan Nacional de Ortofotografía Aérea.
Morgan, R.P.C., 2005. Soil Erosion and Conservation, third ed. Blackwell Science Ltd, Malden, USA.
Morgan, R.P.C., Duzant, J.H., 2008. Modified MMF (Morgan–Morgan–Finney) model for evaluating effects of crops and vegetation cover on soil erosion. Earth Surf. Process. Landf. 33, 90–106. http://dx.doi.org/10.1002/esp.1530.
Morgan, R.P.C., Quinton, J.N., Smith, R.E., Govers, G., Poesen, J.W.A., Auerswald, K., Chisci, G., Torri, D., Styczen, M.E., 1998. The European Soil Erosion Model (EUROSEM): A dynamic approach for predicting sediment transport from fields and small catchments. Earth Surf. Process. Landf. 23, 527–544. http://dx.doi.org/10.1002/(SICI)1096-9837(199806)23:6<527::AID-ESP868>3.0.CO;2-5.
Morianou, G.G., Kourgialas, N.N., Karatzas, G.P., Nikolaidis, N.P., 2018. Assessing hydro-morphological changes in Mediterranean stream using curvilinear grid modeling approach - climate change impacts. Earth Sci. Inform. 11, 205–216. http://dx.doi.org/10.1007/s12145-017-0326-2.
Motayed, A.K., Krishnamurthy, M., 1980. Composite roughness of natural channels. J. Hydraul. Div. 106, 1111–1116. http://dx.doi.org/10.1061/JYCEAJ.0005446.
Mukundan, R., Pradhanang, S.M., Schneiderman, E.M., Pierson, D.C., Anandhi, A., Zion, M.S., Matonse, A.H., Lounsbury, D.G., Steenhuis, T.S., 2013. Suspended sediment source areas and future climate impact on soil erosion and sediment yield in a New York City water supply watershed, USA. Geomorphology 183, 110–119. http://dx.doi.org/10.1016/j.geomorph.2012.06.021.
Nearing, M.A., Foster, G.R., Lane, L.J., Finkner, S.C., 1989. A process-based soil erosion model for USDA-water erosion prediction project technology. Trans. ASAE 32, 1587–1593. http://dx.doi.org/10.13031/2013.31195.
Neverman, A.J., Donovan, M., Smith, H.G., Ausseil, A.-G., Zammit, C., 2023. Climate change impacts on erosion and suspended sediment loads in New Zealand. Geomorphology 427, 108607. http://dx.doi.org/10.1016/j.geomorph.2023.108607.
Peral García, C., Navascués Fernández-Victorio, B., Ramos Calzado, P., 2017. Serie de precipitación diaria en rejilla con fines climáticos. In: Agencia Estatal de Meteorología. http://dx.doi.org/10.31978/014-17-009-5.

Poesen, J., 2018. Soil erosion in the Anthropocene: Research needs. Earth Surf. Process. Landf. 43, 64–84. http://dx.doi.org/10.1002/esp.4250.

Poesen, J.W., van Wesemael, B., Bunte, K., Benet, A.S., 1998. Variation of rock fragment cover and size along semiarid hillslopes: A case-study from Southeast Spain. Geomorphology 23, 323–335. http://dx.doi.org/10.1016/S0169-555X(98)00013-0.

Praskievicz, S., 2015. A coupled hierarchical modeling approach to simulating the geomorphic response of river systems to anthropogenic climate change. Earth Surf. Process. Landf. 40, 1616–1630. http://dx.doi.org/10.1002/esp.3740.

Quansah, C., 1982. Laboratory Experimentation for the Statistical Derivation of Equations for Soil Erosion Modelling and Soil Conservation Design (Ph.D. thesis). Cranfield Institute of Technology.

Renard, K.G., Foster, G.R., Weesies, G.A., McCool, D.K., Yoder, D.C., 1997. Predicting Soil Erosion By Water: A Guide to Conservation Planning with the Revised Universal Soil Loss Equation. RUSLE, pp. 65–100.

Sharafati, A., Pezeshki, E., Shahid, S., Motta, D., 2020. Quantification and uncertainty of the impact of climate change on river discharge and sediment yield in the Dehbar river basin in Iran. J. Soil. Sediments 20, 2977–2996. http://dx.doi.org/10.1007/s11368-020-02632-0.

Shrestha, B., Babel, M.S., Maskey, S., Van Griensven, A., Uhlenbrook, S., Green, A., Akkharath, I., 2013. Impact of climate change on sediment yield in the Mekong River basin: A case study of the Nam Ou basin, Lao PDR. Hydrol. Earth Syst. Sci. 17, 1–20. http://dx.doi.org/10.5194/hess-17-1-2013.

Shrestha, S., Imbulana, N., Piman, T., Chonwattana, S., Ninsawat, S., Babur, M., 2020. Multimodelling approach to the assessment of climate change impacts on hydrology and river morphology in the Chindwin River Basin, Myanmar. CATENA 188, 104464. http://dx.doi.org/10.1016/j.catena.2020.104464.

Shrestha, N.K., Wang, J., 2018. Predicting sediment yield and transport dynamics of a cold climate region watershed in changing climate. Sci. Total Environ. 625, 1030–1045. http://dx.doi.org/10.1016/j.scitotenv.2017.12.347.

Simon, A., Darby, S.E., 2002. Effectiveness of grade-control structures in reducing erosion along incised river channels: The case of Hotophia Creek, Mississippi. Geomorphology 42, 229–254. http://dx.doi.org/10.1016/S0169-555X(01)00088-5.

Switanek, M.B., Troch, P.A., Castro, C.L., Leuprecht, A., Chang, H.-I., Mukherjee, R., Demaria, E.M.C., 2017. Scaled distribution mapping: A bias correction method that preserves raw climate model projected changes. Hydrol. Earth Syst. Sci. 21, 2649–2666. http://dx.doi.org/10.5194/hess-21-2649-2017.

Tangi, M., Schmitt, R., Bizzi, S., Castelletti, A., 2019. The CASCADE toolbox for analyzing river sediment connectivity and management. Environ. Model. Softw. 119, 400–406. http://dx.doi.org/10.1016/j.envsoft.2019.07.008.

Terink, W., Lutz, A.F., Simons, G.W.H., Immerzeel, W.W., Droogers, P., 2015. SPHY v2.0: Spatial processes in HYdrology. Geosci. Model Dev. 8, 2009–2034. http://dx.doi.org/10.5194/gmd-8-2009-2015.

Tollner, E.W., Barfield, B.J., Haan, C.T., Kao, T.Y., 1976. Suspended sediment filtration capacity of simulated vegetation. Trans. ASAE 19, 0678–0682. http://dx.doi.org/10.13031/2013.36095.

Trimble, S.W., 1997. Contribution of stream channel erosion to sediment yield from an urbanizing watershed. Science 278, 1442–1444. http://dx.doi.org/10.1126/science.278.5342.1442.

Vanmaercke, M., Panagos, P., Vanwalleghem, T., Hayas, A., Foerster, S., Borrelli, P., Rossi, M., Torri, D., Casali, J., Borselli, L., Vigiak, O., Maerker, M., Haregeweyn, N., De Geeter, S., Zg\lobicki, W., Bielders, C., Cerdà, A., Conoscenti, C., de Figueiredo, T., Evans, B., Golosov, V., Ionita, I., Karydas, C., Kertész, A., Krása, J., Le Bouteiller, C., Radoane, M., Ristić, R., Rousseva, S., Stankoviansky, M., Stolte, J., Stolz, C., Bartley, R., Wilkinson, S., Jarihani, B., Poesen, J., 2021. Measuring, modelling and managing gully erosion at large scales: A state of the art. Earth-Sci. Rev. 218, 103637. http://dx.doi.org/10.1016/j.earscirev.2021.103637.

Vautard, R., Gobiet, A., Sobolowski, S., Kjellström, E., Stegehuis, A., Watkiss, P., Mendlik, T., Landgren, O., Nikulin, G., Teichmann, C., Jacob, D., 2014. The European climate under a 2 °C global warming. Environ. Res. Lett. 9, 034006. http://dx.doi.org/10.1088/1748-9326/9/3/034006.

Verhaar, P.M., Biron, P.M., Ferguson, R.I., Hoey, T.B., 2010. Numerical modelling of climate change impacts on Saint-Lawrence River tributaries. Earth Surf. Process. Landf. 35, 1184–1198. http://dx.doi.org/10.1002/esp.1953.

Vörösmarty, C.J., Meybeck, M., Fekete, B., Sharma, K., Green, P., Syvitski, J.P., 2003. Anthropogenic sediment retention: Major global impact from registered river impoundments. Glob. Planet. Change 39, 169–190. http://dx.doi.org/10.1016/S0921-8181(03)00023-7.

Wainwright, J., Parsons, A.J., Cooper, J.R., Gao, P., Gillies, J.A., Mao, L., Orford, J.D., Knight, P.G., 2015. The concept of transport capacity in geomorphology. Rev. Geophys. 53, 1155–1202. http://dx.doi.org/10.1002/2014RG000474.

Wang, X., White, M., Tuppad, P., Lee, T., Srinivasan, R., Zhai, T., Andrews, D., Narasimhan, B., 2013. Simulating sediment loading into the major reservoirs in Trinity River Basin. J. Soil Water Conserv. 68, 372–383. http://dx.doi.org/10.2489/jswc.68.5.372.

Williams, J.R., 1975. Sediment-yield prediction with universal equation using runoff energy factor. In: Present and Prospective Technology for Predicting Sediment Yield and Sources. US Department of Agriculture, Agriculture Research Service, Washington DC, pp. 244–252.

Wilson, C., Kuhnle, R., Bosch, D., Steiner, J., Starks, P., Tomer, M., Wilson, G., 2008. Quantifying relative contributions from sediment sources in Conservation Effects Assessment Project watersheds. J. Soil Water Conserv. 63, 523–532. http://dx.doi.org/10.2489/jswc.63.6.523.

Yalin, M.S., 1963. An expression for bedload transportation. J. Hydraul. Div. Proc. Am. Soc. Civ. Eng. 89, 221–250.

Yi, Y., Cheng, X., Yang, Z., Wieprecht, S., Zhang, S., Wu, Y., 2017. Evaluating the ecological influence of hydraulic projects: A review of aquatic habitat suitability models. Renew. Sustain. Energy Rev. 68, 748–762. http://dx.doi.org/10.1016/j.rser.2016.09.138.

Zhang, J., Lin, P., Gao, S., Fang, Z., 2020. Understanding the re-infiltration process to simulating streamflow in North Central Texas using the WRF-hydro modeling system. J. Hydrol. 587, 124902. http://dx.doi.org/10.1016/j.jhydrol.2020.124902.